ANALYSIS OF ACTIVE RUBIDIUM PHOTO-IONIZATION CONCEPT FOR SPACECRAFT SHIELDING FROM HIGH ENERGY NEUTRAL BEAMS

An Undergraduate Research Scholars Thesis

by

ROHAN JILLAPALLI

Submitted to the LAUNCH: Undergraduate Research office at
Texas A&M University
in partial fulfillment of the requirements for the designation as an

UNDERGRADUATE RESEARCH SCHOLAR

Approved by
Faculty Research Advisor: Dr. Christopher Limbach

May 2021

Major: Aerospace Engineering

RESEARCH COMPLIANCE CERTIFICATION

Research activities involving the use of human subjects, vertebrate animals, and/or biohazards must be reviewed and approved by the appropriate Texas A&M University regulatory research committee (i.e., IRB, IACUC, IBC) before the activity can commence. This requirement applies to activities conducted at Texas A&M and to activities conducted at non-Texas A&M facilities or institutions. In both cases, students are responsible for working with the relevant Texas A&M research compliance program to ensure and document that all Texas A&M compliance obligations are met before the study begins.

I, Rohan Jillapalli, certify that all research compliance requirements related to this Undergraduate Research Scholars thesis have been addressed with my Research Faculty Advisor prior to the collection of any data used in this final thesis submission.

This project did not require approval from the Texas A&M University Research Compliance & Biosafety office.

TABLE OF CONTENTS

ABSTRACT

Analysis of Active Rubidium Photo-Ionization Concept for Spacecraft Shielding from High Energy Neutral Beams

Rohan Jillapalli
Department of Aerospace Engineering
Texas A&M University

Research Faculty Advisor: Dr. Christopher Limbach
Department of Aerospace Engineering
Texas A&M University

Recently, a new beamed propulsion concept based on self-guiding of combined laser and particles beams has been proposed for interstellar travel. By firing high velocity neutral rubidium atoms at the spacecraft, speeds up to 7.5% the speed of light could be achieved. One hurdle this project must overcome is how to protect the spacecraft from damage caused by collisions with the high speed particles. A proposed solution is to have the spacecraft generate a magnetic field and have the particles interact with this field rather than the spacecraft directly. Before the particles can be stopped and redirected by the magnetic field, however, they must first be ionized.

This thesis details a modeling study of a two-step photo-ionization process as a means to ionize the incoming flow. To analyze this approach, radiative processes, beam divergence, beam attenuation, and laser/absorption lineshapes were all considered. Additionally, an iterative method was developed to overcome a boundary condition problem that arose due to the unique layout of this mission concept. The final model predicts the percentage of particles that will be ionized before impacting the spacecraft given various mission input parameters.

The initial results showed that with realistic mission parameters the percentage of particles that would be ionized before reaching the spacecraft was too low to adequately protect the space-

craft. The cause for the low ionization percentage was found to be low efficiency ionization using the proposed two-step photo-ionization process. A subsequent study was conducted on alternative ionization schemes using the high energy Rydberg states of the rubidium atom. The results of this study showed that using the Rydberg states could lead to a much more efficient ionization process which in turn could lead to the majority of particles being ionized and stopped by the magnetic field.

DEDICATION

To my family, instructors, peers, and friends who supported me throughout the research process.

ACKNOWLEDGMENTS

Contributors

I would like to thank my faculty advisor, Dr. Christopher Limbach, and my friend and mentor, Hayden Morgan, for their guidance and support throughout the course of this research.

Thanks also go to my friends and colleagues and the department faculty and staff for making my time at Texas A&M University a great experience.

Finally, thanks to my parents and brother for their encouragement, patience, and love.

This research project looked at one aspect of a larger project being investigated at the Laser Diagnostics and Plasma Devices Laboratory at Texas A&M University.

All work conducted for the thesis was completed by the student under the guidance of Dr. Christopher Limbach.

Funding Sources

No funding was received or used to support this project.

NOMENCLATURE

A_{ki}	Einstein A coefficient for spontaneous emission
B_{ik}	Einstein B coefficient for stimulated absorption
B_{ki}	Einstein B coefficient for stimulated emission
c	Speed of light
d_{Exc}	Initial diameter of excitation laser
E_i	Energy of lower state i
E_k	Energy of upper state k
ER	Efficiency ratio
e	Electron charge
f_{ki}	Oscillator strength
g_i	Degeneracy of lower state i
g_k	Degeneracy of upper state k
$g(\nu)$	Lineshape function
h	Planck constant
$\hbar$	Reduced Planck constant
I_{Exc}	Intensity of excitation laser
I_{Ion}	Intensity of ionization laser
k	Boltzmann constant
m_e	Electron rest-mass
N_i	Number density of lower state i
$L(\nu)$	Natural broadened lineshape
$La(\nu)$	Excitation laser lineshape
m	Atomic mass of rubidium particles

N_k	Number density of upper state k
N_{Total}	Total number density
$P_{Abs,Int}$	Power absorbed due to change in intensity
$P_{Abs,Num.Den}$	Power absorbed due to change in number density
R_{Ion}	Rate of ionization
$R_{Sp.Em}$	Rate of spontaneous emission
$R_{St.Abs}$	Rate of stimulated absorption
$R_{St.Em}$	Rate of stimulated emission
$r_{0,Exc}$	Initial radius of excitation laser
r_{Ion}	radium of ionization laser
T	Particle temperature
u_{Rel}	Relative velocity between particles and spacecraft
v_p	Thermal Doppler broadened probable velocity
α	Attenuation coefficient
γ_i	Ionization rate coefficient
ϵ_0	Permittivity of vacuum
Θ	Excitation laser divergence angle
λ_{Exc}	Wavelength of excitation laser
ν	Frequency
ν_L	Excitation laser linewidth
ν_n	Natural broadened linewidth
$\rho(\nu)$	Spectral energy density
σ_i	Photo-ionization cross section
ω_i	Angular frequency
FWHM	Full width half maximum

LDPDL	Laser Diagnostics and Plasma Devices Laboratory
NIAC	NASA Innovative Advanced Concepts
NIST	National Institute of Standards and Technology

1. INTRODUCTION

1.1 Self-Guided Beamed Propulsion Concept

At the Laser Diagnostics and Plasma Devices Laboratory (LDPDL), Dr. Christopher Limbach and graduate student Hayden Morgan are developing an interstellar self-guided beam propulsion system as part of the NASA Innovative Advanced Concepts (NIAC) program [1]. Their idea is to send a beam of high speed rubidium atoms at a spacecraft to achieve speeds as high as 7.5% the speed of light to enable interstellar missions to planets such as Proxima Centauri b. One of the key elements in their concept is a self-guiding effect that is created by overlapping the particle beam with a laser beam. This overlap enables two mutual interactions to take place; optical dipole forces draw the particles into the laser and refraction focuses the laser onto the particles. The resulting hybrid beam is kept narrow and does not diverge over large distances like a pure particle or pure laser beam would as shown in (**Figure 1.1**). This leads to greater momentum transfer to the spacecraft, even when the spacecraft is far away from the beam source. The ability to generate a low diverging beam allows for the propulsion method to be removed from the spacecraft, reducing its mass and power requirements. It is critical to note that in order for the self-guiding effect to take place, the rubidium particles must be neutral (i.e. uncharged).

1.2 Problem Statement: Protecting the Spacecraft

One of the key questions that must be answered before this propulsion concept can be implemented is how do we protect the spacecraft from collisions with the high speed rubidium particles. A proposed solution, offered by NASA engineer Dr. Geoffrey Landis [2], is to generate a magnetic field around the spacecraft and have the particles interact with this field rather than the spacecraft directly. Before the rubidium particles can be stopped by the magnetic field, they must be ionized. The particles, however, must be neutral as they propagate towards the spacecraft to ensure the self-guiding effect remains. This conflict necessitates an ionization method that can occur close enough to the spacecraft to prevent the beam from diverging too much but far enough

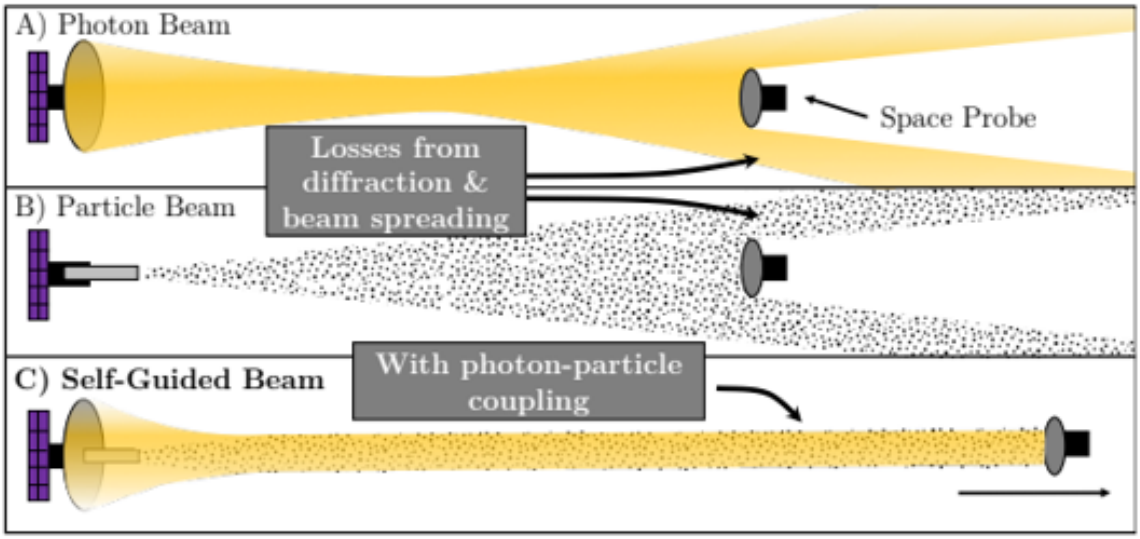

Figure 1.1: Self-guided beam compared with pure particle and pure laser beams.

away from the spacecraft to allow sufficient time for the ionization process to take place. The goal of the research presented in this thesis is to model the process of rubidium ionization by an on-board laser and predict the percentage of particles that can be ionized before collision with the spacecraft.

1.3 Two-Step Photo-Ionization

To ionize the rubidium particles, enough energy must be provided to excite them from the atomic ground state to above the ionization threshold. A method known as photo-ionization will be used to provide energy to the neutral, ground state rubidium atoms [3]. If we used a one-step photo-ionization scheme, a single deep ultraviolet laser would be needed, which is not available. In addition, the laser would consume too much power for a feasible mission concept. Instead, a two-step photo-ionization scheme was chosen in which the ionization process is split into two parts. First, one laser provides enough energy to excite the particles from the starting ground state to an intermediate excited state. Then, a second laser provides enough energy to excite the particles from this intermediate excited state to the ionization continuum [3]. This process can be seen in (**Figure 1.2**). In our mission, the first step will be carried out by a small laser mounted on-board the spacecraft. The second step will be carried out be the overlapped guiding laser that is propagating

with the rubidium particles. This arrangement can be seen in (**Figure 1.3**).

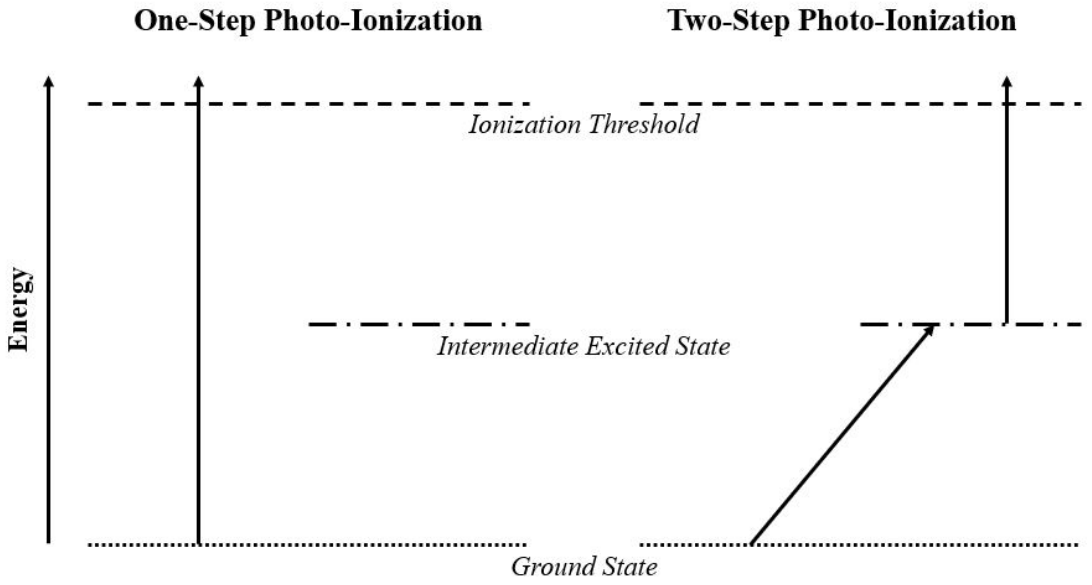

Figure 1.2: Photo-ionization scheme comparison.

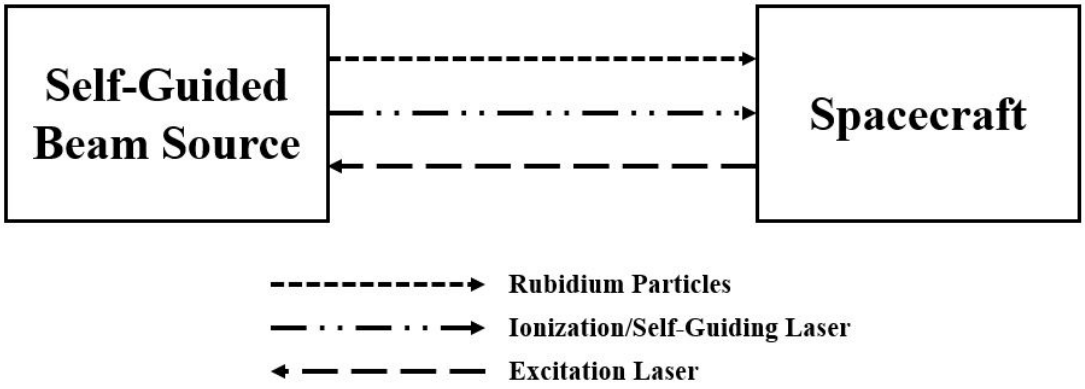

Figure 1.3: Two-step photo-ionization laser and particle arrangement.

2. METHODS

In this section, the methods used to create the rubidium ionization model will be described. At this point, it is important to note that two different transitions to the intermediate excited state were examined: the 780.0 nm transition to the $5P_{3/2}$ state and the 420.2 nm transition to the $6P_{3/2}$ state. As seen in (**Figure 2.1**), the 780.0 nm transition has a more simple, 3-level energy diagram compared to the 7-level 420.2 nm transition. Therefore, the two-step photo-ionization process was modeled using the 780. nm transition first. The 420.2 nm transition was considered because of the higher energy intermediate excited state. The mission concept uses a 1 micron high power laser to achieve self-guiding. This wavelength is too high to ionize from the $5P_{3/2}$ but is sufficient to ionize from the $6P_{3/2}$ level. Once the model was working with the simpler 780.0 nm case, the 420.2 nm case was implemented. In this section, a general notation will be used to describe the methods as they were identical for both the 780.0 and 420.2 nm transitions. The differing results of the two transitions are presented and discussed in the **Results** section.

2.1 Rate Equations

To begin modelling the two-step photo-ionization method we must consider the radiative processes the rubidium particle can use to transition between different states. Through stimulated absorption, ionization, stimulated emission and spontaneous emission, the rubidium particles can populate and vacate different levels. The direction of each radiative process can be seen in (**Figure 2.1**). When all the processes are summed together, a system of equations can be created that describe the number density of each state as a function of time. These equations are called Rate equations.

2.1.1 Stimulated Absorption

When a particle undergoes stimulated absorption it *absorbs* a photon from the excitation laser and moves from the ground state to the intermediate excited state [4]. The amount of energy

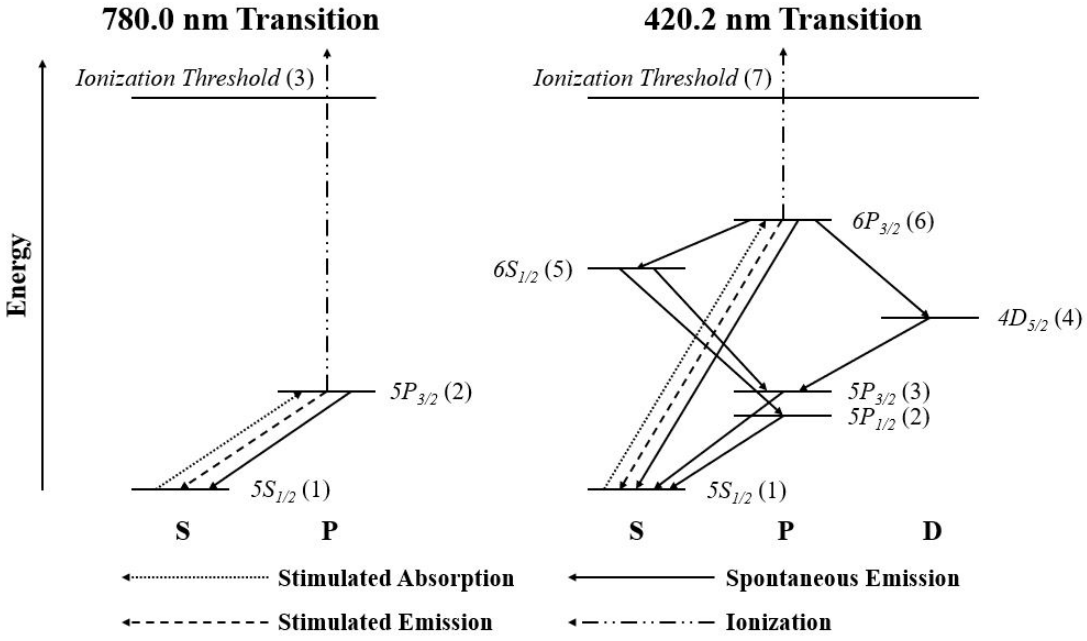

Figure 2.1: Energy diagrams for the 780.0 and 420.2 nm transitions.

that is absorbed depends on the frequency of the photon as seen in the following equation:

$$E_k - E_i = h\nu \qquad \text{(Eq. 1)}$$

where E_k and E_i are the energies of the upper and lower states respectively and ν is the frequency of the absorbed photon.

The rate at which stimulated absorption populates the intermediate excited state is given by the following equations:

$$R_{St.Abs} = B_{ik}\rho(\nu)N_i \qquad \text{(Eq. 2)}$$

$$B_{ik} = \frac{g_k}{g_i}B_{ki} \qquad \text{(Eq. 3)}$$

$$\rho(\nu) = \int \frac{g(\nu)I_{Exc}}{c}\,d\nu \qquad \text{(Eq. 4)}$$

where B_{ik} is the Einstein B coefficient for stimulated absorption, B_{ki} is the Einstein B coeffcient for stimulated emission, g_k and g_i are the degeneracies of the upper and lower states respectively, $\rho(\nu)$ is the spectral energy density, N_i is the number density of the lower state, $g(\nu)$ is the lineshape function, and I_{Exc} is the excitation laser intensity.

2.1.2 Ionization

Ionization is similar to stimulated absorption, however, the photon that is absorbed comes from the ionization/self-guiding laser rather than the excitation laser. The rate at which particles are ionized from the intermediate excited state is given by the following equations [5]:

$$R_{Ion} = \gamma_i N_i \tag{Eq. 5}$$

$$\gamma_i = \frac{\sigma_i I_{Ion}}{\hbar \omega_i} \tag{Eq. 6}$$

where γ_i is the ionization rate coefficient, σ_i is the photo-ionization cross-section, and ω_i is the angular frequency from the intermediate excited state i. I_{Ion} is the intensity of the ionization laser.

2.1.3 Stimulated Emission

Stimulated emission occurs when an atom that is already in the excited state encounters a photon from the excitation laser [4]. The result is that the excited particle will release a photon of energy of equal frequency to the encountered photon. The particle will decay back down to the ground state and the 2 photons of energy will return to the excitation laser.

The rate at which stimulated emission occurs is given by the following equation:

$$R_{St.Em} = B_{ki} \rho(\nu) N_k \tag{Eq. 7}$$

where N_k is the number density of the upper state.

2.1.4 Spontaneous Emission

The final radiative process, spontaneous emission, occurs when a particle in one of the excited states *spontaneously* releases a photon is a random direction [4]. The result is that the particle will decay to either a lower excited state, or to the ground state if no transition to a lower excited state exists. Unlike in stimulated emission, the photon of energy that is releases does not go back to the excitation laser. Instead, the photon of energy is considered lost from the system.

The rate at which spontaneous emission occurs is given by the following equations:

$$R_{Sp.Em} = A_{ki} N_k \tag{Eq. 8}$$

$$A_{ki} = 8\pi h \frac{\nu^3}{c^3} B_{ki} \tag{Eq. 9}$$

where A_{ki} is the Einstein A coefficient.

The majority of Einstein A coefficients were taken from the National Institute of Standards and Technology (NIST) Atomic Spectra Database [6]. The Einstein B coefficients were then calculated from these values using Eq. 9. However, not all of the Einstein A coefficients were listed on NIST. The missing coefficients were calculated using oscillator strength data that was tabulated in a paper by Miles and Harris [7]. Using the oscillator strengths, the missing Einstein A coefficient can be calculated using the following equation [8]:

$$f_{ki} = \frac{\epsilon_0 m_e c^3}{2\pi \nu_{ki}^2 e^2} A_{ki} \tag{Eq. 10}$$

where f_{ki} is the oscillator strength.

2.1.5 System of Ordinary Differential Equations

With a method to calculate the rate for the four radiative processes, we can construct the system of differential equations governing the excitation dynamics. These equations are valid so long as the atomic response or excitation laser is incoherent [9]. The number of differential equations is equal to the number of states in the system. Therefore, the 780.0 nm transition will have

three equations, and the 420.0 nm transition will have 7 equations. Each equation is constructed by adding the rates of each radiative process that populates the state and subtracting the rates of each radiative process that vacates the state. For example, (**Figure 2.1**) shows that State 6 for the 420.2 nm transition has 1 radiative process populating it and 5 radiative processes vacating it. Therefore, the rate equation for State 6 is given by the following:

$$\frac{dN_6}{dt} = B_{16}\rho(\nu)N_1 - A_{65}N_6 - A_{64}N_6 - A_{61}N_6 - B_{61}\rho(\nu)N_6 - \gamma_i N_6 \qquad \text{(Eq. 11)}$$

Repeating this process for each state yields a system of ordinary differential equations which when solved simultaneously, gives the number density of each state as a function of time. It is worth noting that an additional equation can be constructed from the conservation of the total number of rubidium particles. For future calculations, it would be more convenient if the equations produced the number density of each state as a function of position. To do this, a constant relative velocity between the rubidium particles and the spacecraft, u_{Rel}, is assumed. This approximation is valid because the beam is mono-energetic and the overlapped laser provides negligible additional acceleration. Using the constant relative velocity, the new differential equations can be calculated as the following:

$$\frac{dN_i}{dx} = \frac{dN_i}{dt}\, u_{Rel}^{-1} \qquad \text{(Eq. 12)}$$

Solving the new system of differential equations will yield the number density as a function of position as desired.

2.2 Excitation Laser Divergence

Now that the number densities of each state can be calculated, we can consider the decrease in laser intensity as a function of position. This decrease in the intensity of the excitation laser can be attributed to two sources: divergence and attenuation.

The excitation laser, which is mounted on board the spacecraft as shown in (**Figure 1.3**), does not benefit from the self-guiding effect like the ionization laser. This results in the excitation laser diverging as it propagates away from the spacecraft and towards the rubidium particles. This

increase in area leads to a decrease in laser intensity as shown in (**Figure 2.2**). The angle of divergence can be approximated with the following equations:

$$\Theta = \frac{\lambda_{Exc}}{d_{Exc}} \qquad \text{(Eq. 13)}$$

Where λ_{Exc} is the wavelength of the excitation laser and d_{Exc} is the initial diameter of the excitation laser. It is important to note that the decrease in excitation laser intensity due to divergence is solely due to an increase in area and not on a decrease in power.

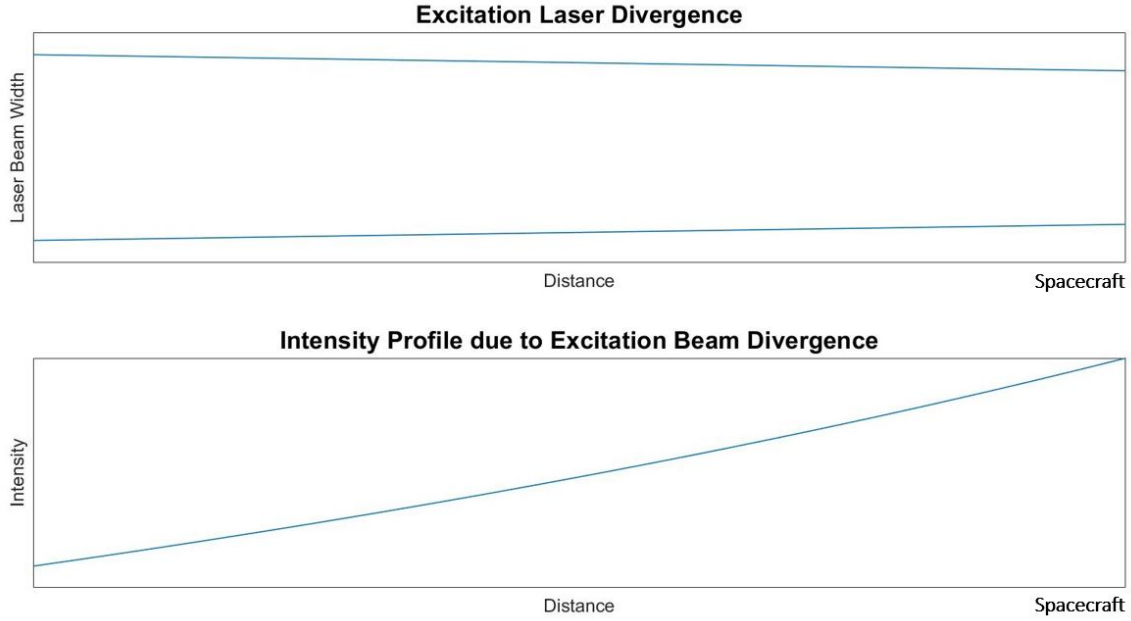

Figure 2.2: Excitation laser divergence. Laser is propagating from right to left.

2.3 Excitation Laser Attenuation

2.3.1 Beer-Lambert Law

Another cause for the decrease in excitation laser intensity comes from a loss in power. As the excitation laser passes through the ground state rubidium atoms, it will attenuate power to excite the particles to an intermediate state. The resulting intensity profile can be calculated using

the Beer-Lambert Law:

$$\frac{dI_{Exc}}{I_{Exc}} = -\alpha(x)dx \qquad \text{(Eq. 14)}$$

$$\alpha(x) = -(N_k(x) * B_{ki} - N_i(x) * B_{ik})(g(\nu) * \frac{h\nu}{c}) \qquad \text{(Eq. 15)}$$

where α is the attenuation coefficient.

It can be seen from Eq. 14, and Eq. 15 that in order to calculate the intensity profiles, we must first know the number density profiles across the region of interest. Looking at Eq. 4 and Eq. 11, however, it can also be seen that the number density profiles depend on the intensity profiles. This mutual dependence between the number density and intensity profiles suggests that the two need to be calculated simultaneously. Next, we consider the proper specification of the boundary conditions needed to solve these equations.

2.3.2 Boundary Condition Problem

As shown in (**Figure 1.3**), the rubidium particles and the excitation laser propagate in opposite directions. Therefore, the rate equations are posed with initial data on the left side of the domain, whereas the laser initial data is on the right boundary. That is, the number density profiles are calculated using the rate equations from left to right whereas the intensity profiles are calculated using the Beer-Lambert law from right to left. The boundary condition for the rate equations is known on the left side where we assume all particles begin in the ground state. The boundary condition for the Beer-Lambert Law is known on the right side as the initial intensity of excitation laser before divergence or attenuation. This can be seen in (**Figure 2.3**). Therefore, there does not exists a point in the spatial domain in which both the number density and intensity are known. This makes it impossible to solve the rate equations and the Beer-Lambert Law directly to obtain the desired number density and intensity profiles.

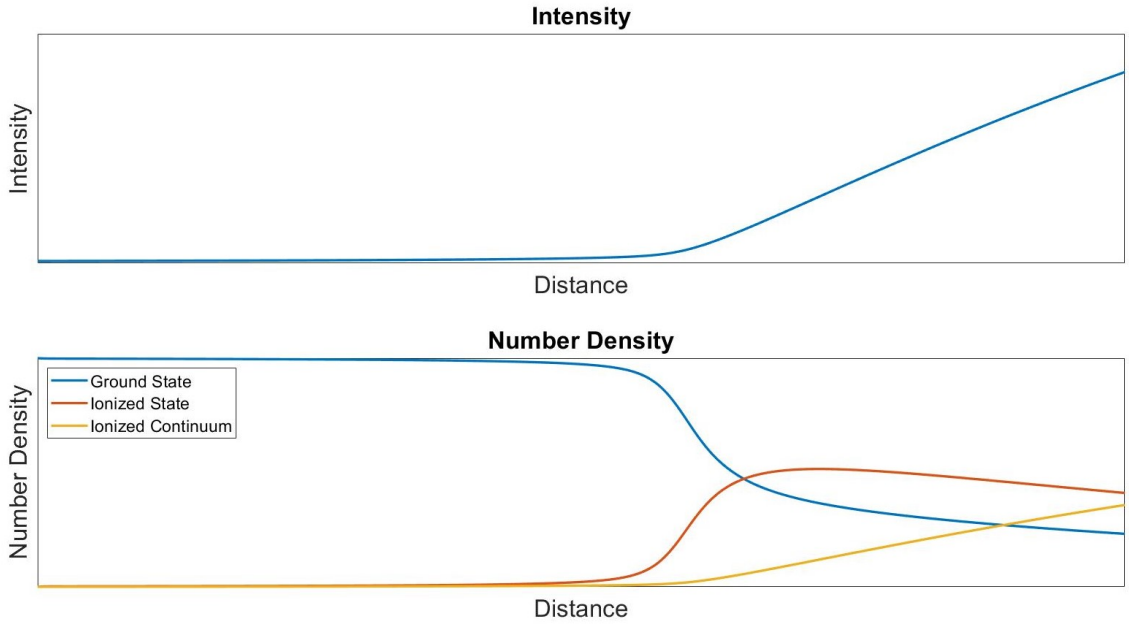

Figure 2.3: Counter-propagating intensity and number density profiles.

2.3.3 Iterative Method

To overcome the boundary condition problem, an iterative method was developed to determine the intensity and number density profiles. The steps of the process are listed:

1. Make a guess for the intensity profile.
2. Use the intensity profile to solve for the spectral energy density.
3. Use spectral energy density to solve the rate equations and obtain the number density profiles.
4. Use number density profiles to solve for the attenuation coefficient.
5. Use the attenuation coefficient to solve the Beer-Lambert Law for an updated intensity profile.
6. Return to Step 2.

The results of this iterative method is an intensity profile that converges to a solution with self-consistent density and intensity profiles as seen in (**Figure 2.4**). (**Figure 2.5**) shows how the intensity profile of each subsequent iteration converges. Using the converged intensity profile, the rate equations can be solved to obtain the number densities of each state.

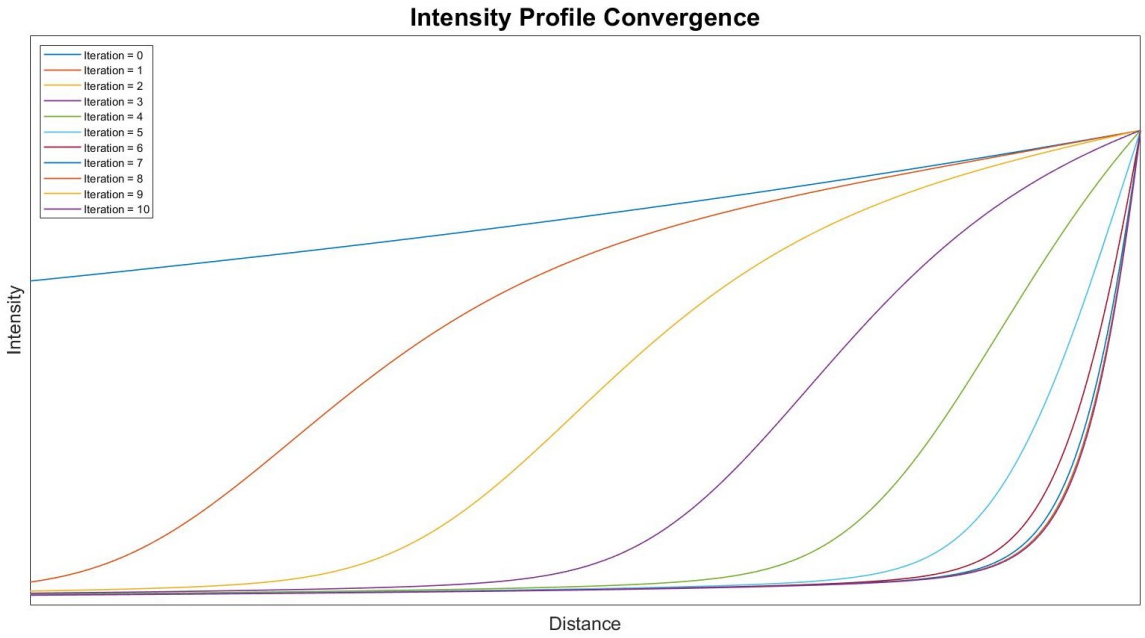

Figure 2.4: Intensity profiles after ten iterations.

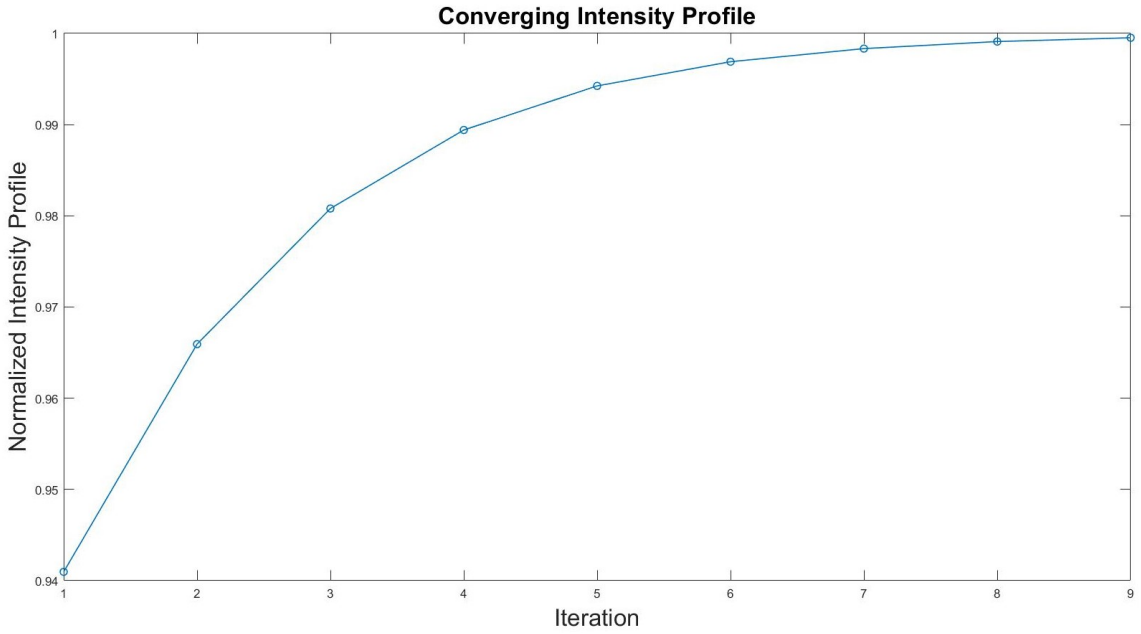

Figure 2.5: Normalized intensity profile convergence.

2.4 Lineshapes

To correctly model the frequency dependent interaction between the excitation laser and the rubidium particles, we must implement the lineshapes of each. When the excitation laser is tuned to the atomic transition frequency, not every photon will be at precisely the same frequency. Instead, some portion of the photons will be at a higher frequency and some portion will be at a lower frequency. Similarly, when stimulated absorption occurs, it is possible that a ground state particle absorbs a photon of energy, even if the exciting photon is not precisely at the atomic transition frequency. The interaction of these two lineshape functions can describe the frequency dependent excitation of the atomic beam and the attenuation of the laser beam, both of which are critical in analyzing the effectiveness of the ionization scheme.

2.4.1 Excitation Laser Lineshape

Though it would be ideal if every photon emitted from the laser was at the tuned frequency, the reality is that the laser will operate over a narrow range of frequencies. The distribution of the excitation laser photons over the range of frequencies is described with a Lorentzian lineshape [4]:

$$La(\nu) = \frac{\Delta\nu_L}{2\pi[(\Delta\nu)^2 + (\Delta\nu_L/2)^2]} \qquad \text{(Eq. 16)}$$

where $\Delta\nu_L$ is the full width half maximum (FWHM) of the excitation laser. The Lorenztian lineshape has a maximum value at the center and decreases as the distance from the center frequency increases. One key element of the lineshape is it must be normalized. That is to say, integrating the Lorentzian lineshape over frequency should return unity. By using the Lorentzian function to model the laser beam in terms of frequency and including the spatial divergence of the laser beam, a spatial and frequency dependent model of the laser beam can be constructed. This true laser intensity profile is then used to evaluate the interaction of the excitation system with the atomic beam. Lastly, the effects of laser beam attenuation due to the excitation of rubidium atoms can be taken into account to accurately model the decay in laser intensity in both the spatial and frequency domains.

2.4.2 Absorption Lineshape

The absorption lineshape is less trivial than the excitation laser as it is the convolution of two lineshapes caused by two different broadening mechanisms: natural and thermal Doppler broadening. Natural broadening is caused by the variation in lifetimes of the particles in the excited state. When the particle decays back to a lower energy state, the frequency of the photon emitted can occur over a range of values. The natural broadened lineshape is also modelled using a Lorentzian lineshape [4]:

$$L(\nu) = \frac{\Delta\nu_n}{2\pi[(\Delta\nu)^2 + (\Delta\nu_n/2)^2]} \qquad \text{(Eq. 17)}$$

This time, however, the FWHM, $\Delta\nu_n$, is calculated using the sum of the spontaneous emission coefficients from the excited state:

$$\Delta\nu_n = \frac{1}{2\pi}\sum A_{ki} \qquad \text{(Eq. 18)}$$

As before, the lineshape must be normalized.

The second absorption broadening mechanism is thermal Doppler broadening. Doppler broadening stems from the velocity distribution of the atoms in the jet. The direction of motion the atom is traveling in relative to the laser propagation vector at the moment of excitation is what yields the Doppler shift. The typical Doppler broadening mechanism is the velocity distribution stemming from the temperature of the atoms. The Doppler broadened lineshape can be described with a Gaussian profile [3]:

$$F(\nu) = \frac{\lambda_{Exc}}{\pi^{1/2} v_p} e^{-\left(\frac{\Delta\nu}{v_p/\lambda_{Exc}}\right)^2} \qquad \text{(Eq. 19)}$$

$$v_p = \sqrt{2kT/m} \qquad \text{(Eq. 20)}$$

where v_p is the most probably velocity T is the temperature and m is the atomic mass of the

particles. As with the Lorentzian lineshapes, the Gaussian lineshapes must also be normalized. Though other broadening mechanisms exist, they are negligible in the context of this mission.

A convolution of the natural broadening Lorentzian profile and the Doppler broadening Gaussian profile is necessary to describe their contributions to the absorption profile. The combination of these two broadening mechanisms yields the Voigt profile. This Voigt profile is then used in comparison with the laser lineshape to model atom excitation and laser attenuation.

2.5 Energy Conservation

Energy conservation is calculated to ensure that the obtained results provide a self-consistent description of the excitation process. To check for energy conservation, we consider the power absorbed through a control volume as seen in (**Figure 2.6**). The power absorbed can be calculated with both the number density and intensity profiles using the following equations:

$$P_{Abs,Num.Den} = (B_{ki}N_k - B_{ik}N_1)(\rho(\nu))(h\nu) \quad \text{(Eq. 21)}$$

$$P_{Abs,Int.} = \frac{I(x-dx) - I(x)}{dx} \quad \text{(Eq. 22)}$$

The power absorbed due to the number density described the energy required to move the ground state particles into the intermediate excited state. The power absorbed due to the intensity describes the energy lost in the excitation laser to carry out the transition. If energy is conserved, these two power absorbed values should be equal.

The energy conservation check for the 780.0 nm case is shown in (**Figure 2.7**). The relative error between the power absorbed calculated through the Beer-Lambert Law and the rate equations does not exceed 1.5%.

The energy conservation check for the 420.2 nm case is shown in (**Figure 2.8**). The relative error between the power absorbed calculated through the Beer-Lambert Law and the rate equations is 23.28%.

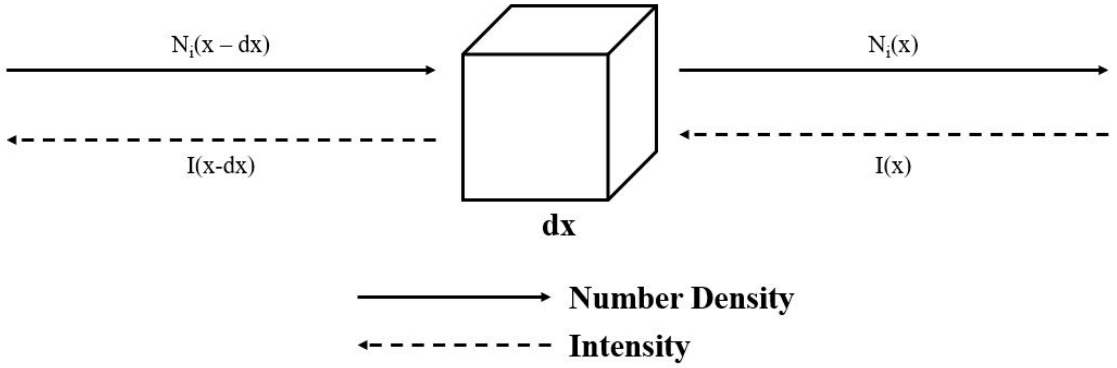

Figure 2.6: Power absorbed control volume.

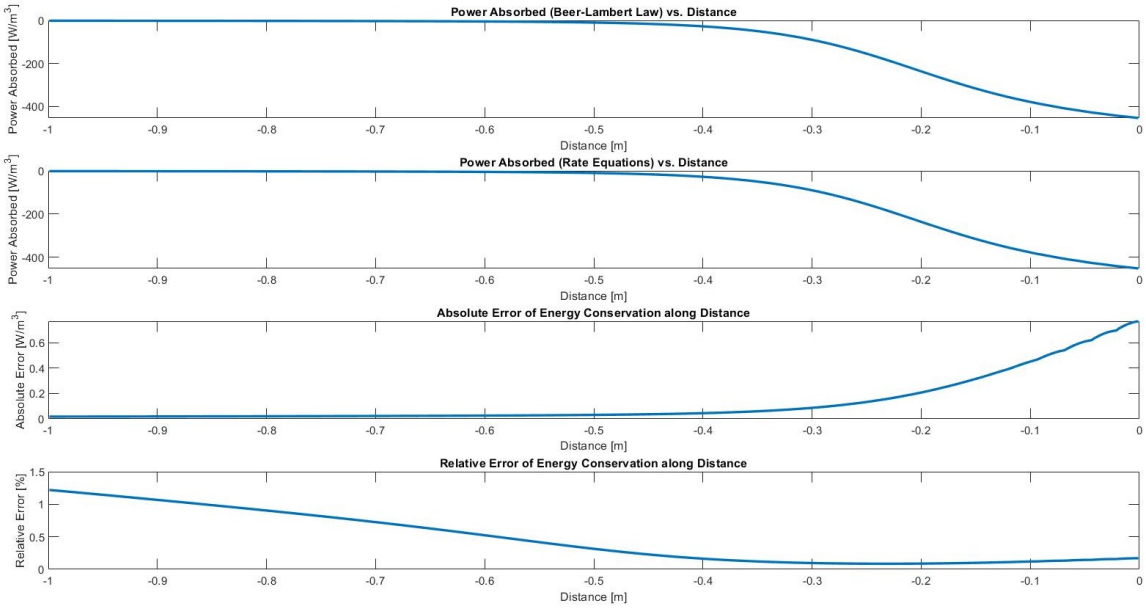

Figure 2.7: 780.0 nm transition power absorbed energy conservation check.

2.6 Rydberg States

The results of the model, which are presented in detail in the **Results** section, showed that with the standard two-step photo-ionization scheme the percentage of particles that would be ionized before reaching the spacecraft was insufficient. The cause for the low ionization percentage was determined to be a low efficiency ionization. Once particles were in the intermediate excited state, the majority would decay back down to the the ground state through spontaneous emission

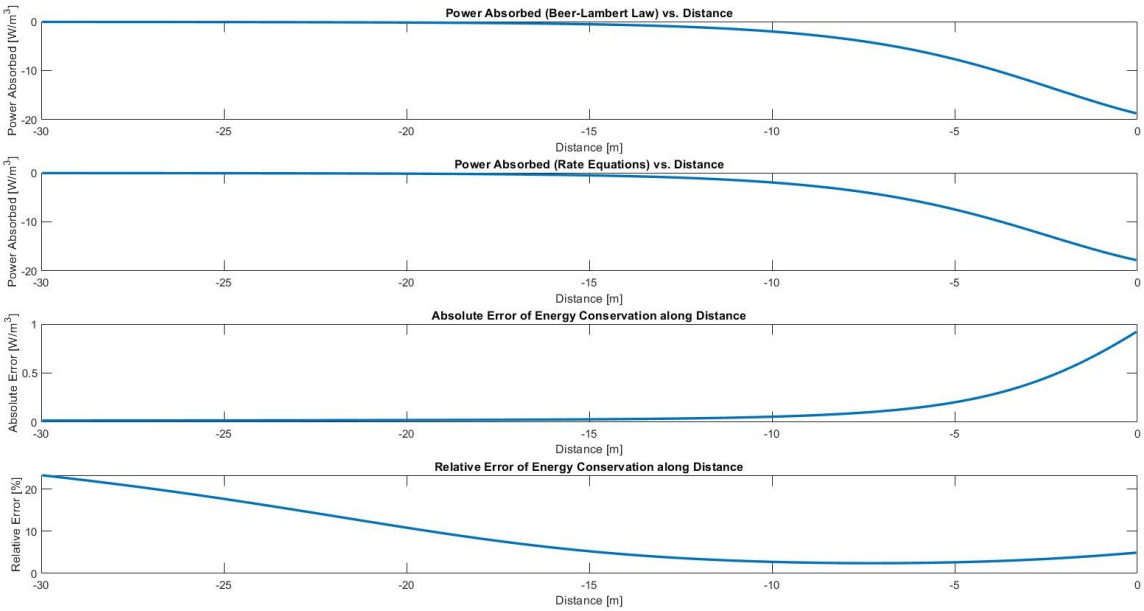

Figure 2.8: 420.2 nm transition power absorbed energy conservation check.

rather than be promoted up past the ionization threshold. This process can be described by a parameter we define:

$$ER = \frac{\gamma_i}{\sum A_{ki}} \qquad \text{(Eq. 23)}$$

where ER is the efficiency ratio of the ionization process.

To increase to the ionization percentage, we wish to increase the efficiency ratio. This lead to a study on the high energy Rydberg states of the rubidium atom. Rydberg states are energy states that exist very close to the ionization threshold. The two advantages of these states are a high threshold ionization cross-section which increases in the ionization coefficient and a high probable lifetime which leads to a low probability of spontaneous emission.

The effectiveness of the Rydberg states was studied using a model to calculate the probable lifetime and ionization cross-sections at each energy level [10]. This model is based on quantum defect theory [11] in which alkali-metals are treated as expanded hydrogen atoms. The results of the model showed that a higher efficiency ratio, and thus higher ionization percentage, could be achieved using the d-orbital Rydberg states. These results can be seen in the (**Results**) section.

3. RESULTS

In this section, the results of the developed rubidium ionization model will be presented. Two transitions were examined: 780.0 nm and 420.0 nm. After presenting and discussing the results of each transition, the results of the Rydberg model [10] will be discussed.

3.1 780.0 nm Transition

As mentioned previously, the 780.0 nm transition was studied first due to its simple 3-state model. The proposed mission calls for a guiding laser with a frequency close to 1 micron. This frequency is too low to ionize from the $5P_{3/2}$ state. Nevertheless, the results of this transition are still useful and help validate the methods used for modelling desired 420.2 nm transition.

One of the main purposes of the model was to act as a design tool in which various mission input parameters could be entered. The following results are calculated using the mission input parameters found in (**Table 3.1**).

Table 3.1: Mission Input Parameters for the 780.0 nm Transition

Parameter	**Value**
I_{Exc}	100 $[W/m^2]$
I_{Ion}	10^9 $[W/m^2]$
$Iterations$	30
N_{Total}	10^{14} $[1/m^3]$
$r_{0,Exc}$	0.01 $[m]$
r_{Ion}	0.4 $[m]$
u_{Rel}	1000 $[km/s]$
λ_{Exc}	780.0 $[nm]$
λ_{Ion}	479.0 $[nm]$
ν_L	1 $[GHz]$

The intensity of the 780.0 nm transition attenuates very quickly. It can be seen in (**Figure 3.1**) that the intensity of laser is near zero after propagating less than 0.4 meters from the spacecraft.

We can also see that the intensity of the laser is highest at the center frequencies and attenuate quickly as you move outwards.

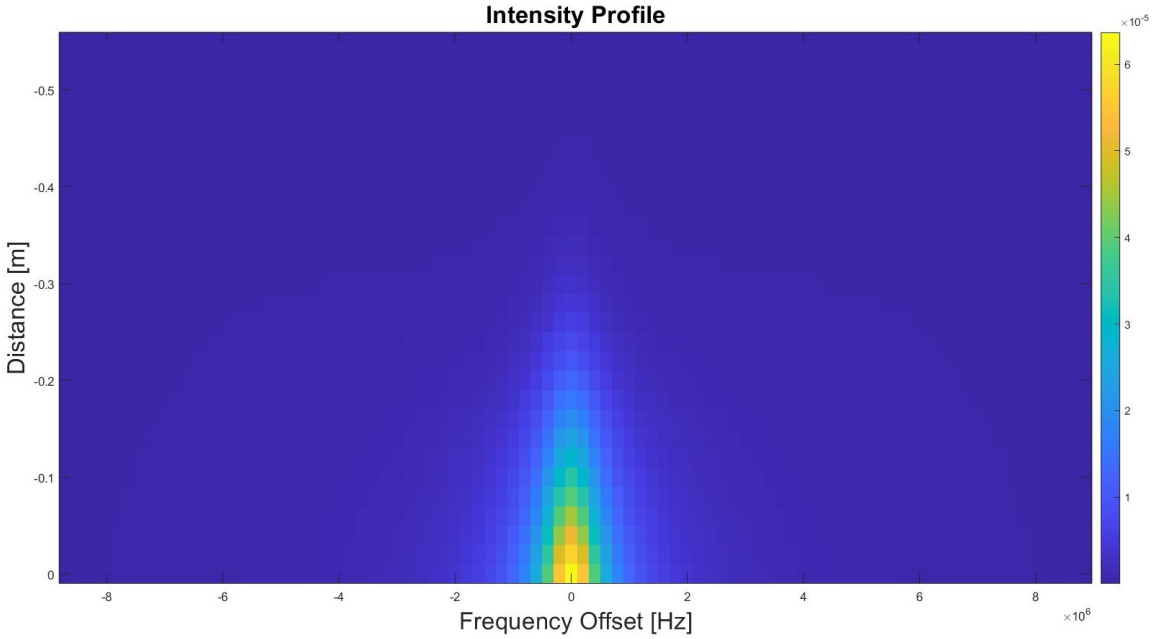

Figure 3.1: 780.0 nm transition intensity profile.

This rapid attenuation of the excitation laser is reflected in the number density profiles shown in (**Figure 3.2**). The ground state rubidium particles do not undergo stimulated emission that is consequential to the dynamics of the spacecraft until very close to the spacecraft where the intensity of the excitation laser is substantial. Because the excitation process does not begin occurring until very close to the spacecraft, there is insufficient time for meaningful ionization to take place. The result is that only 3.1841% of the starting rubidium particles are ionized before impact with the spacecraft. The efficiency ratio of the process is only 0.0095. In other words, for every 1 rubidium particle that undergoes ionization, approximately 100 particles undergo spontaneous emission and decay back down to the ground state.

Though not the primary transition of interest, the 780.0 nm transition shows us that with the realistic mission input parameters, the two-step photo-ionization method is highly inefficient.

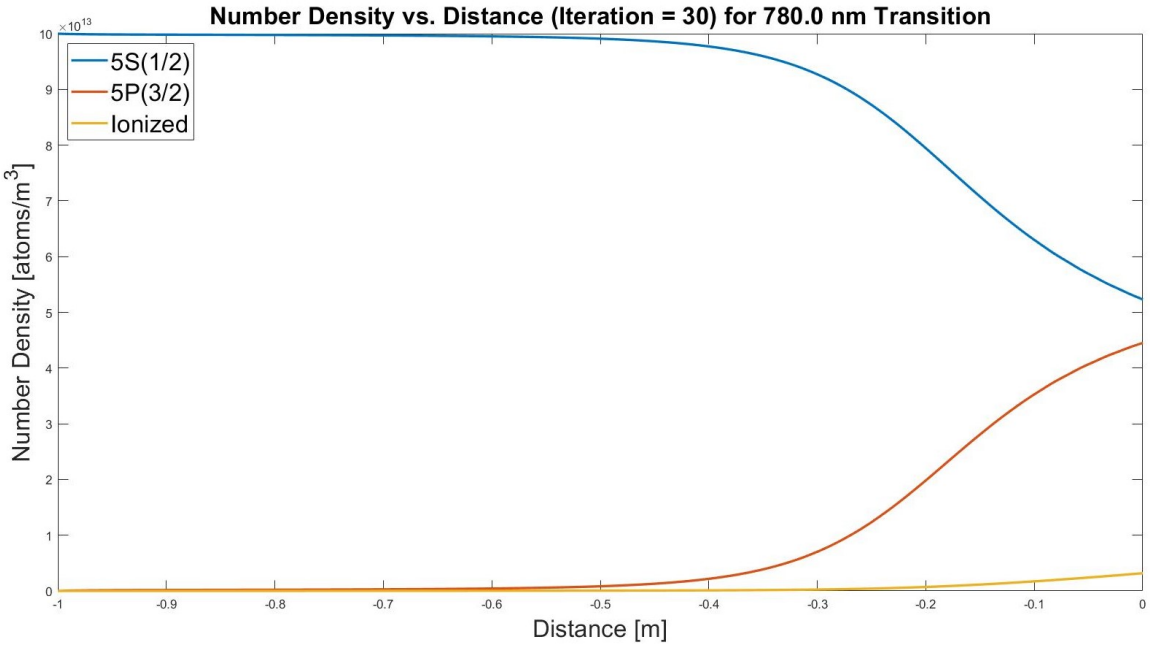

Figure 3.2: 780.0 nm transition number density profile.

3.2 420.2 nm Transition

For the mission, the 420.2 nm transition was the most desirable due to the higher energy of the $6P_{3/2}$ excited state. From this state, an ionization laser with a wavelength of 1 micron is capable of energizing the excited particles up past the ionization threshold. Therefore, the results of the 420.2 nm transition were of highest relevance and interest. The following results are calculated using the mission input parameters found in (**Table 3.2**).

The excitation laser intensity attenuation for 420.0 nm transition is much less than the for the 780.0 nm transition. (**Figure 3.3**) shows that the laser attenuates to near zero intensity after propagating 18 meters from the spacecraft. This is over an order of magnitude greater than the 780.0 nm case.

The lower attenuation means that excitation and ionization can occur earlier leading to an improved ionization percentage as shown in (**Figure 3.4**). The attenuation, however, is still too high to ionize the majority of the rubidium particles. With the mission input parameters, an ionization percentage of 31.188% was obtained. The efficiency ratio of this process was 0.1945.

Table 3.2: Mission Input Parameters for the 420.2 nm Transition

Parameter	**Value**
I_{Exc}	100 $[W/m^2]$
I_{Ion}	10^9 $[W/m^2]$
$Iterations$	30
N_{Total}	10^{14} $[1/m^3]$
$r_{0,Exc}$	0.01 $[m]$
r_{Ion}	0.4 $[m]$
u_{Rel}	1000 $[km/s]$
λ_{Exc}	420.2 $[nm]$
λ_{Ion}	1000 $[nm]$
ν_L	1 $[GHz]$

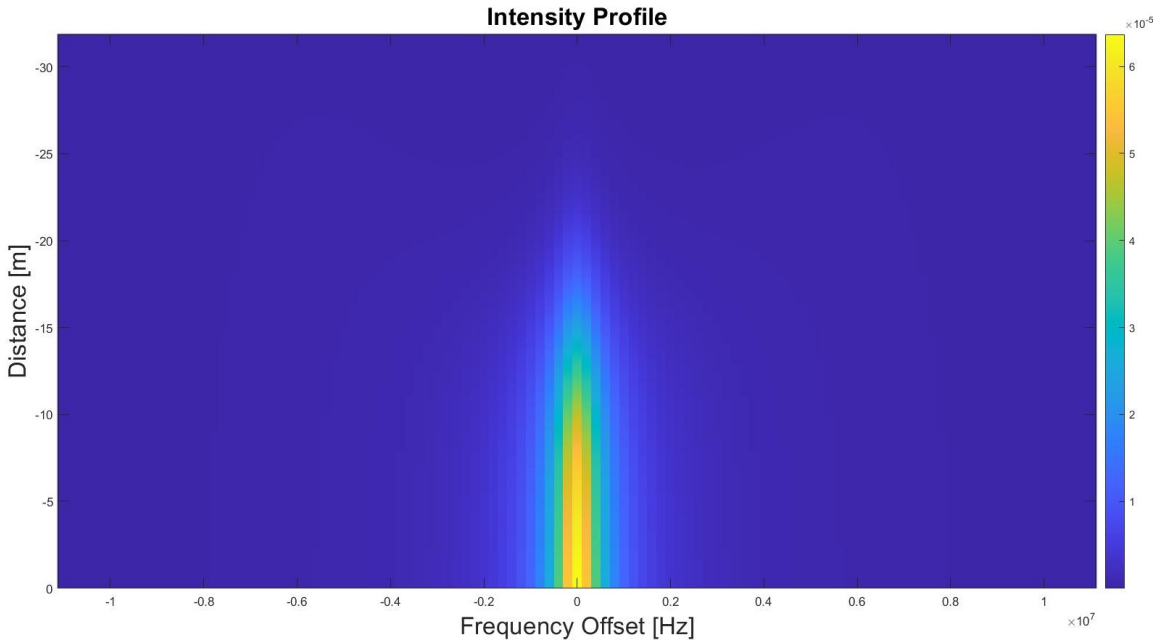

Figure 3.3: 420.2 nm transition intensity profile.

This means that for every excited particle that is ionized, approximately 5 particles decay back down to the ground state. Again, these result are much better than the 780.0 nm case but are still lower than what we would like to successfully protect the spacecraft.

The results for the 420.2 nm case show that though we get an improved ionization percentage of 31.2%, we are still not ionizing efficiently enough the increase that percentage to where we

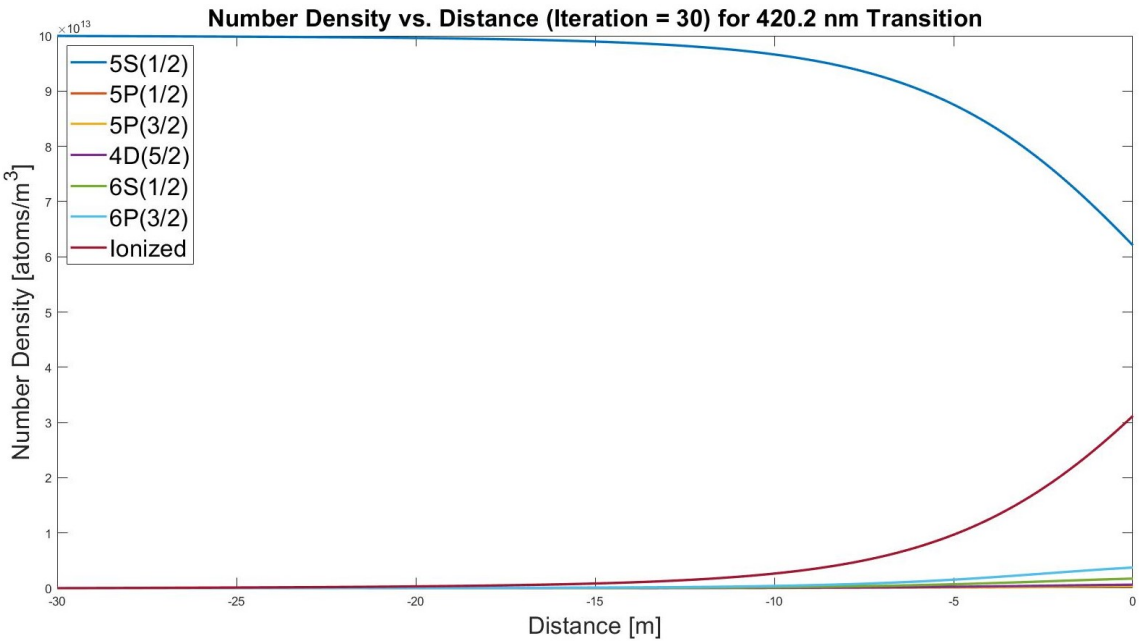

Figure 3.4: 420.2 nm transition number density profile.

would like. To confirm that low efficiency ionization was the cause of the low ionization percentage, the efficiency ratio was artificially increased to 1. The result, shown in (**Figure 3.5**), was an ionization percentage of 92.493%. This leads us to believe that if we are able to identify a more efficient ionization process, majority ionization is still possible using photo-ionization.

3.3 Rydberg States Study

A possible method of increasing the efficiency ratio by using the high energy Rydberg states was identified. These states are characterized by a low probability of spontaneous emission and a high ionization cross-section leading to a high probability of ionization. The results of the adapted rubidium Rydberg model [10] are shown in (**Figure 3.6**). Two different ionization wavelengths are considered. The 1 micron wavelength was studied because it is the current wavelength of the guiding laser. The 1.5 micron wavelength was studied to observe the effects of increasing the ionization wavelength. The efficiency ratio of the S- and P-orbitals are lower than the ratio of the 420.2 nm transition. This suggests they would not be useful for increasing the ionization percentage. The D-orbital, however, has greatly increased efficiency ratios. For principal quantum

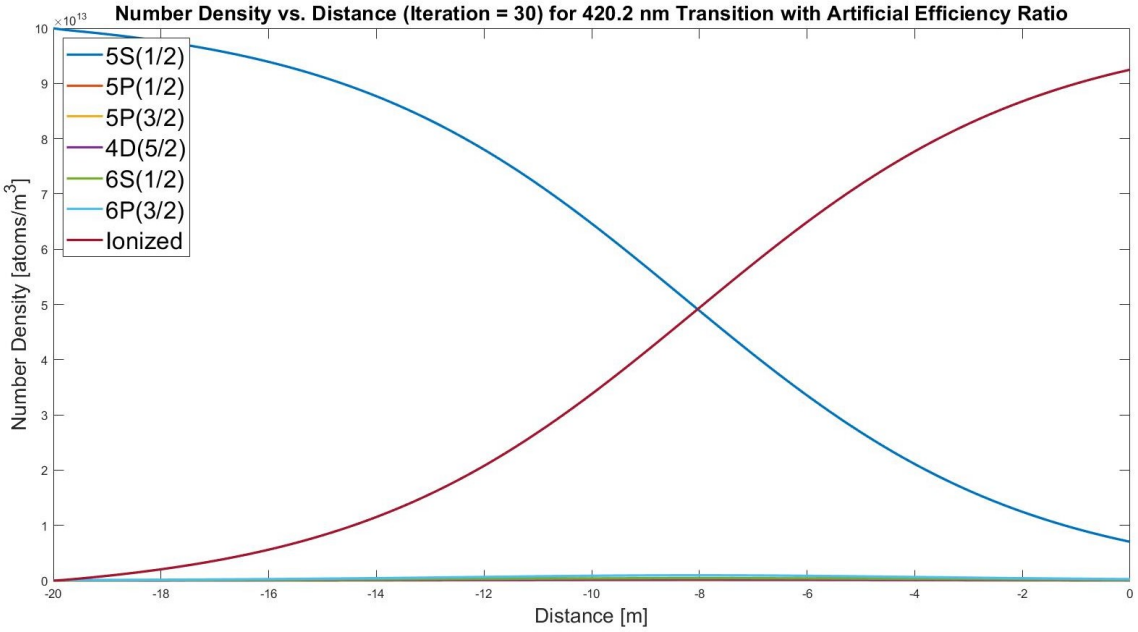

Figure 3.5: 420.2 nm transition number density profile with artificial efficiency ratio.

numbers between 10 and 20, the efficiency ratio of the D-orbital is greater than 1. The results of this model have not been verified with experimental data. If accurate, however, the results indicate an ionization scheme using D-orbital Rydberg levels would provide the highest efficiency.

It is important to note that the efficiency ratios shown in (**Figure 3.6**) cannot be directly compared to the efficiency ratio reported for the 420.2 nm case because it is not possible to ionize ground state rubidium particles from the D-orbital using two-step photo-ionization. If the D-orbitals are to be used, they would require a more complicated ionization setup, likely involving two excitation lasers. The large efficiency ratios of the D-orbitals, however, are quite motivating. It is possible that this more complicated ionization process could yield the high ionization percentage needed to successfully protect the spacecraft.

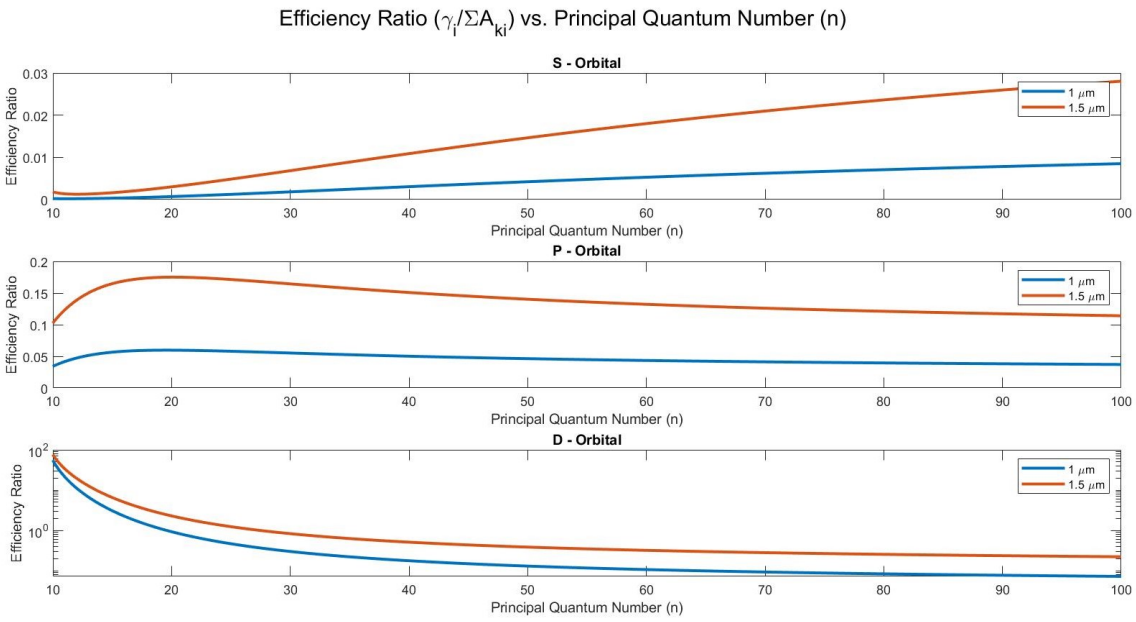

Figure 3.6: Efficiency ratio from Rydberg excited states.

4. CONCLUSION

The self-guiding beamed propulsion system currently being developed could enable amazing mission farther than we have ever gone before. For these mission to be successful, it is vital that the spacecraft not be destroyed by the propulsion system. The work presented in this thesis examined a proposed solution to help protect the spacecraft from the high speed rubidium particles.

A two-step photo-ionization model was created to determine if enough rubidium particles would be ionized before impact with the spacecraft. Rate equations were implemented to describe the rate at which each state was populated and vacated. The beam divergence and the Beer-Lambert Law were used to describe the decrease excitation laser intensity as it spreads and energized the ground state rubidium particles respectively. Lineshapes were added to accurately model the frequency dependent interaction between the excitation laser and the absorption feature. Finally, the energy conservation was checked using the power absorbed from both the rate equations and the Beer-Lambert Law. The results showed that though ionization was possible, the final ionization percentage of 31.2% allowed too many neutral particles to by pass the magnetic field and impact the spacecraft. The reason for the low ionization percentage was attributed to the low efficiency ratio of the two-step photo-ionization method.

In response, a study was performed on the high energy Rydberg states using a model based on quantum defect theory. Though the results have not yet be verified, they showed that if ionization occurred from a high energy D-orbital state, the efficiency of the ionization process could be orders of magnitude greater than what we were obtaining with a standard two-step photo-ionization method. Certainly, the results warrant further investigation as this could be the key to increasing the ionization percentage and allowing the interstellar spacecraft to be protected by the generated magnetic field.

REFERENCES

[1] C. Limbach and K. Hara, "PROCSIMA: Diffractionless Beamed Propulsion for Breakthrough Interstellar Missions," pp. Report No. HQ–E–DAA–TN67917, 2019.

[2] G. A. Landis, "Interstellar Flight by Particle Beam," in *STAIF Conference on Innovative Transportation Systems for Exploration of the Solar System and Beyond*, (Albuquerque), 2001.

[3] W. Demtröder, *Laser Spectroscopy: Basics Concepts and Instrumentation*. Springer, 3 ed., 2003.

[4] L. S. Pedrotti, L. M. Pedrotti, and F. L. Pedrotti, *Introduction to Optics*. Cambridge University Press, 3 ed., 2018.

[5] G. Ten Haaf, S. H. Wouters, P. H. Mutsaers, and E. J. Vredenbregt, "Cavity-enhanced photoionization of an ultracold rubidium beam for application in focused ion beams," *Physical Review A*, vol. 96, no. 5, pp. 1–12, 2017.

[6] A. Kramida, Y. Ralchenko, J. Reader, and NIST ASD Team (2020), "NIST Atomic Spectra Database Lines Data (Rubidium)."

[7] R. B. Miles and S. E. Harris, "Optical Third-Harmonic Generation in Alkali Metal Vapors," *IEEE Journal of Quantum Electronics*, vol. 9, no. 4, pp. 470–484, 1973.

[8] R. K. Hanson, M. R. Spearrin, and C. S. Goldenstein, *Spectroscopy and Optical Diagnostics for Gases*. Springer, 2016.

[9] R. Höppner, E. Roldán, and G. J. de Valcárcel, "A semiclassical optics derivation of Einstein's rate equations," *American Journal of Physics*, vol. 80, no. 10, pp. 882–890, 2012.

[10] V. D. Ovsiannikov, I. L. Glukhov, and E. A. Nekipelov, "Radiative lifetime and photoionization cross-section for Rydberg states in alkali-metal atoms," *Optics and Spectroscopy (English translation of Optika i Spektroskopiya)*, vol. 111, no. 1, pp. 25–33, 2011.

[11] M. J. Seaton, "Quantum defect theory," *Reports on Progress in Physics*, vol. 46, no. 2, pp. 167–257, 1983.